

Metal–Organic Framework-Templated Catalyst: Synergy in Multiple Sites for Catalytic CO₂ Fixation

Meili Ding,^[a] Si Chen,^[a] Xiao-Qin Liu,^[b] Lin-Bing Sun,^[b] Junling Lu,^[a] and Hai-Long Jiang^{*[a, b]}

The types and quantities of active sites play a critical role in catalysis. Herein, ZnO nanoparticles encapsulated into N-doped porous carbon has been rationally prepared by the pyrolysis of a metal–organic framework (MOF) followed by a moderate oxidation treatment. The resulting catalyst exhibits excellent activity, selectivity, and recyclability in the CO₂ cycloaddition reactions with epoxides owing to the synergy of multiple sites inherited from the MOF and generated by the oxidation process.

In recent years, ocean acidification, global warming, and many environmental issues caused by greenhouse gases (GHGs) have attracted growing attention. As the primary source of GHGs, CO₂ comes mainly from the burning of fossil fuels and its concentration was reported to be over 400 ppm in atmospheric air by 2015.^[1] On the other hand, CO₂ is actually an economical, abundant, renewable, and nontoxic C1 source providing value-added chemicals, such as formic acid, cyclic carbonate, and carbon monoxide.^[2] One of the main challenges for CO₂ utilization is the high kinetic and thermodynamic stability of the CO₂ molecule, which requires a large amount of energy to activate.^[2a,b,3] In this context, the concentrated CO₂ molecules around active sites would facilitate its conversion. Therefore, it is highly desirable to develop cost-effective and efficient strategies to integrate CO₂ capture and conversion (C3).

Among various strategies developed for the catalytic CO₂ transformation, the cycloaddition of CO₂ and epoxides to cyclic carbonates is very promising, not only because of its atom economy and green chemistry but also owing to the high valued-added products.^[4] So far, different types of catalysts were reported for the CO₂ cycloaddition reaction, for example, metal complexes, ionic liquids, and alkali metal salts.^[2d,4] In addition, compared with traditional homogeneous catalysts, the heterogeneous catalysts, such as metal–organic frameworks

(MOFs) and porous polymers, are attracting great interest on account of the bifunction of CO₂ capture and simultaneous catalytic conversion.^[2c,9,5] In contrast, porous carbons possessing high surface area, excellent stability, and low density, are promising candidates but rarely reported for catalytic CO₂ conversion.^[6] The major reasons behind this should be the lack of active sites and the weak interactions between CO₂ molecules and carbon materials. To address these issues, three characteristics of carbon materials are of great importance: i) a moderately high surface area with suitable pore sizes would be beneficial to the exposure of active sites and transport of reaction substrates/products; ii) polar functional sites/groups grafted onto the pore walls are desirable to improve the interaction between the framework and CO₂ molecules,^[1a,7] iii) active sites available for substrates and CO₂ are necessary. Based on previous reports, different acids, such as phenolic hydroxyl and carboxyl groups, ZnO species, etc., and Lewis bases such as pyridinic N, can be effective active sites.^[6c,8] Particularly, the integration of acid and base sites into a single catalyst is favorable for the conversion of CO₂ by cycloaddition.^[8e]

On the other hand, MOFs have been demonstrated to be ideal templates/precursors to afford uniform metal (oxide) particles distributed throughout porous carbon with high surface areas by facile pyrolysis.^[6f,9] Among all MOFs, ZIF-8 (also called MAF-4, Zn(MeIM)₂, MeIM = 2-methylimidazole)^[10] as a representative MOF, possesses an intersecting 3D structure with pore size of 11.6 Å, high N content, ZnN₄ node, and large Brunauer–Emmett–Teller (BET) surface area (1413 m²g⁻¹), which has been widely used as template and precursor to prepare N-doped porous carbon or carbon-based composites for diverse applications, particularly in catalysis.^[9]

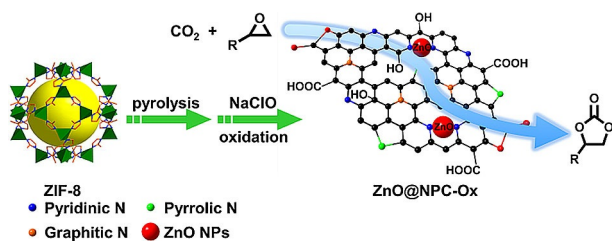
Bearing the above points in mind, the generation of multi-components in the resulting composite from ZIF-8 pyrolysis might evoke a synergetic effect between the components and endow the catalyst with superior catalytic performance for the CO₂-fixation reaction. Herein, the ZIF-8 precursor was pyrolyzed and subsequently oxidized by sodium hypochlorite to produce ZnO nanoparticles (NPs) encapsulated into N-doped porous carbon (ZnO@NPC-Ox) (Scheme 1), which includes carboxylic acid, phenol, and lactone functional groups on the surface of the porous carbon, given the moderate oxidation ability of sodium hypochlorite.^[11] Remarkably, the resultant composite exhibits efficient conversion toward CO₂ cycloaddition under mild conditions (60 °C, 0.1 MPa CO₂), on account of the synergetic effect of multiple catalytic sites involving ZnO species, pyridinic N, hydroxyl, and carboxyl groups in the oxidative porous carbon matrix (Scheme 1).

The ZIF-8 nanocrystals were synthesized by simply stirring a mixture of Zn(NO₃)₂·6H₂O and 2-methylimidazole in metha-

[a] M. Ding, S. Chen, Prof. Dr. J. Lu, Prof. Dr. H.-L. Jiang
Hefei National Laboratory for Physical Sciences at the Microscale
CAS Key Laboratory of Soft Matter Chemistry
Collaborative Innovation Center of Suzhou Nano Science and Technology
School of Chemistry and Materials Science,
University of Science and Technology of China
Hefei, Anhui 230026 (P. R. China)
E-mail: jianglab@ustc.edu.cn
Homepage: <http://staff.ustc.edu.cn/~jianglab/>

[b] Prof. Dr. X.-Q. Liu, Prof. Dr. L.-B. Sun, Prof. Dr. H.-L. Jiang
State Key Laboratory of Materials-Oriented Chemical Engineering
College of Chemistry and Chemical Engineering
Nanjing Tech University
Nanjing, Jiangsu 210009 (P. R. China)

Supporting Information and the ORCID identification number(s) for the author(s) of this article can be found under <http://dx.doi.org/10.1002/cssc.201700245>.



Scheme 1. Illustration showing the preparation of ZIF-8-templated ZnO@NPC-Ox toward CO₂ cycloaddition with epoxides.

nol at room temperature. The obtained ZIF-8 as both a template and a precursor underwent pyrolysis at different temperatures in N₂ atmosphere to afford the ZnO NPs encapsulated into N-doped porous carbon (denoted ZnO@NPC-*T*, with *T* representing the pyrolysis temperature, *T* = 700, 800, 900, or 1000 °C), which were further oxidized by NaClO to give ZnO@NPC-Ox-*T*.

The phase purity of ZIF-8 was confirmed by powder X-ray diffraction (PXRD) (Figure S1 in the Supporting Information). Upon pyrolysis, the PXRD patterns of all products show a weak broad peak at approximately 25°, which should be assigned to the typical (002) diffraction of graphitic carbon. The rest of the identifiable peaks in the pyrolysis products obtained at 700 and 800 °C can be indexed to wurtzite (ZnO, JCPDS NO. 36-1451) (Figure S2). In contrast, the corresponding peaks of ZnO species were not present in the products at 900 and 1000 °C because ZnO could be reduced by carbon to generate evaporative Zn at such high temperatures.^[9b,d,e,12] After the oxidation treatment with NaClO, the intensity of the PXRD peaks indexed to ZnO species significantly decrease in ZnO@NPC-Ox-700 and the peaks almost disappeared in ZnO@NPC-Ox-800 (Figure 1 a). The porous character and surface area of all materials were investigated by N₂ sorption at 77 K. The original ZIF-8 shows relatively high surface area (1235 m²g⁻¹) and microporous charac-

ter (Figure S3). Upon pyrolysis, the resultant porous carbon composites partially inherit the pore character of ZIF-8 with relatively high BET surface area (403–1963 m²g⁻¹, Figure S4 a). The BET surface area of ZnO@NPC-Ox-*T* significantly decreases compared to the above composites, owing to the oxidation of the carbon matrix (Figure S5 a). Moreover, the pyrolysis temperature is crucial to the BET surface area of the composites before and after the oxidation treatment. In addition, the steep rise of the sorption curves and the hysteresis loop at relatively high pressure (*P*/*P*₀ = 0.9–1.0) manifest the presence of mesopores and macropores in these materials, which were further verified by the pore-size distribution analysis based on the density functional theory (DFT) method (Figure S4 and S5). To demonstrate the reproducibility of these samples, three batches of ZnO@NPC-Ox-700, as a representative sample, were investigated and they displayed almost the same pore structures and properties (Figure S6). Although the BET surface areas of ZnO@NPC-Ox-*T* were not very high (77–150 m²g⁻¹), the hierarchical pores, especially macropores, are suited to expose the catalytic sites and transfer substrates and products. Based on the porosity and the suspended polar functional groups (hydroxyls and carboxyls) on the pore walls, the oxidized products exhibit moderate CO₂-uptake capacity (20–34 mg g⁻¹) at 273 K (Figure S7), which would be important for the subsequent CO₂ cycloaddition reaction.

The successful introduction of oxygen surface groups on ZnO@NPC-Ox was confirmed by Fourier transform infrared (FTIR) spectroscopy, with ZnO@NPC-Ox-700 as representative sample (Figure 1 b). The broad peak at 3400 cm⁻¹ corresponds to the stretching vibration of the O–H bonds from hydroxyl and carboxyl groups,^[13a,b] which were absent in the spectrum of ZnO@NPC-700. The C=O stretching band of lactone is approximately 1820 cm⁻¹ and the strong peak at 1650 cm⁻¹ is also attributed to the vibration of C=O.^[13b,c] The band at 1600 cm⁻¹ is assigned to the vibration of carbon skeleton.^[13a,b,d] In addition, the characteristic peaks at 1420, 1368, 1100, and 1048 cm⁻¹ of ZnO@NPC-Ox-700 come from the C–O stretching (carboxyl), O–H deformation, C–O–C stretching (lactone), and C–O stretching (alkoxy), respectively.^[13d–g] In contrast to ZnO@NPC-Ox-700, the carbon composite oxidized by HNO₃ (ZnO@NPC-700-HNO₃) shows a peak around 1725 cm⁻¹ assignable to the stretching vibration of C=O (carboxyl) (Figure S8).^[13a,d] All of these observations reveal that the oxidation from sodium hypochlorite results in carboxylic acid, phenol, and lactone functional groups on the pore surface of ZnO@NPC-Ox-700 and the main functional group in ZnO@NPC-700-HNO₃ is carboxyl, all of which are consistent with previous reports.^[11,14]

The morphology and microstructure of ZIF-8, the porous carbon composites, and their oxidized products were observed, with ZnO@NPC-700 and ZnO@NPC-Ox-700 as the representative samples, respectively, by SEM and TEM. In comparison with the polyhedral ZIF-8 nanocrystals in 70–80 nm, ZnO@NPC-700 and its oxidized product retain the morphology of ZIF-8 with slightly reduced sizes (~50 nm) (Figure S9). The TEM and high-resolution TEM (HRTEM) images demonstrate that the ZnO NPs are well dispersed within ZnO@NPC-Ox-700

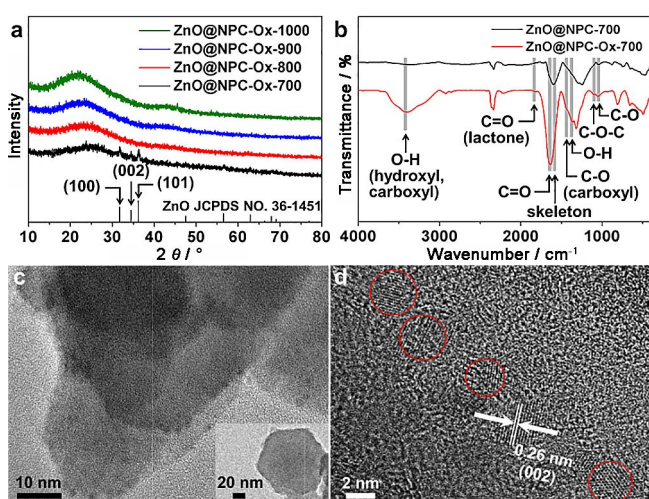


Figure 1. a) PXRD patterns of ZnO@NPC-Ox-*T* composites (*T* = 700, 800, 900, or 1000 °C). b) FTIR spectra of ZnO@NPC-700 and ZnO@NPC-Ox-700 catalysts. c) TEM and d) HRTEM images of ZnO@NPC-Ox-700. Inset in c): enlarged single ZnO@NPC-Ox-700 particle.

with average sizes of approximately 3 nm (Figure 1 c,d). The lattice fringes with an interplanar spacing of 0.26 nm correspond to the (002) plane of ZnO, which is consistent with the PXRD results (Figure 1 a).

To further understand the existing form of the Zn and N species in ZnO@NPC-Ox-T composites, X-ray photoelectron spectroscopy (XPS) was investigated. The high-resolution XPS spectra for N 1s reveal two types of N species in ZnO@NPC-Ox-T ($T=700, 800$): pyridinic N (398.7 eV) and pyrrolic N (400.3 eV) (Figures 2a and S10a).^[6a,15] When the calcination temperature

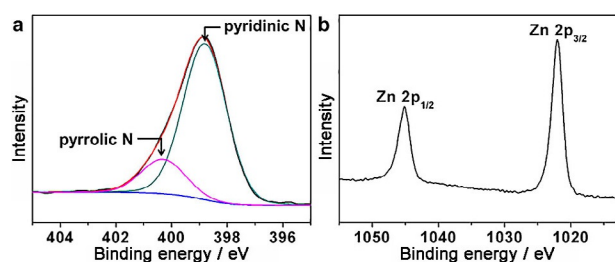
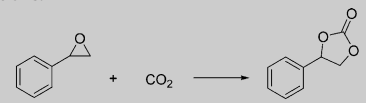


Figure 2. XPS spectra of high-resolution a) N 1s and b) Zn 2p for ZnO@NPC-Ox-700.

was further elevated, the most stable nitrogen (graphitic N) appears and increases, accompanying with the decrease of the overall N content (from 11.18 wt% in ZnO@NPC-Ox-700 to 4.19 wt% in ZnO@NPC-Ox-1000) (Figure S10b,c and Table S1). The Zn 2p spectra in all ZnO@NPC-Ox samples show similar peaks, suggesting their similar chemical states (Figure 2b and S11). The two broad peaks at 1021.8 and 1044.5 eV can be assigned to Zn 2p_{3/2} and 2p_{1/2}, respectively.^[9] The peak distance of 22.7 eV is similar to that reported for ZnO and the content of Zn dramatically decreased with the increase of pyrolysis temperature, which is also supported by the above-mentioned PXRD results (Figure 1 a).

Encouraged by the multiple catalytic sites and hierarchical pores in ZnO@NPC-Ox, CO₂ cycloaddition with styrene oxide was first chosen as a model catalytic reaction to evaluate the catalytic properties of the composites (Table 1). Among all ZnO@NPC-Ox samples, ZnO@NPC-Ox-700 possesses the highest conversion (98%) and selectivity (100%), in the presence of tetrabutyl ammonium bromide (TBAB), to give the target product phenylethylene carbonate under mild conditions (60 °C, 0.1 MPa CO₂) (entries 1–4). The catalytic efficiency of different batches of ZnO@NPC-Ox-700 was almost the same, suggesting the reproducible activity (Table S2). Evidently, the presence of ZnO and high-content pyridinic N in ZnO@NPC-Ox-700 are responsible for the efficient conversion (Figure 2 and Table S1), whereas pyrrolic and graphitic N are almost inessential because of the lack of Lewis basicity.^[6a] We need to stress that both the catalyst and co-catalyst (TBAB) are indispensable for the efficient conversion of CO₂ (Table 1, entries 5–6). In reference to TBAB, tetrabutyl ammonium chloride (TBAC) only leads to 34% conversion, probably because of the strong constraint of the quaternary ammonium ion for the chloride ion with small radius (entry 7).^[16] Unexpectedly, when ZIF-8 and TBAB were

Table 1. Catalytic CO₂ cycloaddition reaction of styrene oxide under different conditions.^[a]



Entry	Catalyst	Con. ^[b] [%]	Sel. ^[b] [%]
1	ZnO@NPC-Ox-700 + TBAB	98	100
2	ZnO@NPC-Ox-800 + TBAB	94	100
3	ZnO@NPC-Ox-900 + TBAB	89	100
4	ZnO@NPC-Ox-1000 + TBAB	87	100
5	TBAB	14	100
6	ZnO@NPC-Ox-700	< 1	100
7 ^[c]	ZnO@NPC-Ox-700 + TBAC	34	100
8	ZIF-8 + TBAB	16	100
9	ZnO@NPC-700 + TBAB	77	100
10 ^[d]	ZnO + TBAB	43	100
11 ^[e]	ZnO@NPC-Ox + TBAB	85	100
12 ^[f]	ZnO@AC + TBAB	59	100
13 ^[g]	NPC-Ox-700 + TBAB	50	100
14 ^[h]	ZnO@NPC-700-HNO ₃ + TBAB	56	100
15 ^[i]	ZnO@NPC-Ox-700-HNO ₃ + TBAB	58	100

[a] Reaction conditions: 1 mmol styrene oxide, 50 mg catalyst, 0.2 mmol TBAB, 2 mL acetonitrile, 0.1 MPa CO₂, 60 °C, 2 d. [b] Determined by GC and using *n*-dodecane as standard. [c] 0.2 mmol TBAC. [d] Catalyst: 6.9 mg ZnO pyrolyzed from ZIF-8 in air (calculated by the actual content of Zn in ZnO@NPC-Ox-700). [e] Catalyst: 50 mg ZnO@NPC-Ox. [f] Catalyst: 50 mg ZnO@AC. [g] Catalyst: 43.1 mg NPC-Ox-700. [h] Catalyst: 50 mg ZnO@NPC-700-HNO₃. [i] Catalyst: 50 mg ZnO@NPC-Ox-700-HNO₃.

used, the conversion (16%) was almost similar to the that of pure TBAB (14%), indicating the low reactivity of ZIF-8 under such conditions (entry 8), possibly owed to the lack of sufficient active sites and/or the small apertures of ZIF-8 (3.4 Å). Notably, although ZIF-8 might be able to host larger molecules than its pore aperture owing to the mobility of linkers, the reaction would be considerably restricted because of the low diffusion rates.^[17] To demonstrate the significance of multiple catalytic sites in ZnO@NPC-Ox-700, control experiments were conducted. As expected, when ZnO@NPC-Ox-700 was replaced by ZnO@NPC-700 or ZnO pyrolyzed from ZIF-8 in air, the conversion of substrates sharply lowered to 77 and 43%, respectively (entries 9–10, Figure S13). As only two types of active sites in ZnO@NPC-700 (pyridinic N and ZnO) and the single active site in pure ZnO, these results reflect the contribution of hydroxyl, carboxyl, and pyridinic N sites to CO₂ fixation. In addition, the benefits of ZnO obtained by pyrolysis of ZIF-8 over conventional ZnO encapsulated into porous carbon have been further illustrated by control experiments with ZnO@NPC-Ox and ZnO@AC (AC = activated carbon) catalysts (see Experimental Section; Figure S14). These two catalysts present 85 and 59% yields (entries 11–12), respectively, in reference to the higher yield of ZnO@NPC-Ox-700 (entry 1). Therefore, the ZnO obtained by pyrolysis of ZIF-8 possesses superior activity than the conventional ZnO encapsulated into porous carbon, possibly owing to the small sizes, good dispersity, and interactions between ZnO and diverse functional groups on the surface of ZnO@NPC-Ox-700. Interestingly, the activity of ZnO@AC (entry 12) is slightly higher than ZnO (entry 10), which is proba-

bly because of the aggregation of ZnO NPs in the latter. When NPC-Ox-700 was employed as a catalyst, approximately 50% substrate could be converted to the target product, demonstrating that the NPC-Ox-700 support is also active for the CO₂ cycloaddition of styrene oxide (entry 13, Figure S15).

To understand the critical step of the mild oxidation, ZnO@NPC-700 was oxidized in 1 M HNO₃ solution to give ZnO@NPC-700-HNO₃. This strong oxidation treatment mainly results in carboxylic acids on the pore surface of carbon and most of ZnO in the carbon would be etched off, supported by the above-mentioned FTIR results, the disappearance of PXRD peaks for ZnO and the result of inductively coupled plasma atomic emission spectroscopy (ICP-AES) (Figures S8 and S16, and Table S3).^[11,14] Unfortunately, the resultant product showed only 56% conversion after 2 days under similar conditions (Table 1, entry 14). For further comparison, the ZnO@NPC-Ox-700 was also treated in 1 M HNO₃ solution to give ZnO@NPC-Ox-700-HNO₃. Such treatment results in not only the disappearance of the PXRD characteristic peaks of ZnO but also the reduced conversion to 58% (Table 1, entry 15, Figure S16, and Table S3). These results imply that the great activity of ZnO@NPC-Ox-700 is ascribed to the synergy of the multiple catalytic sites involved and that NaClO is an ideal oxidant for the post-synthetic oxidation compared to a traditional strong oxidant such as HNO₃. In addition to the activity, as a heterogeneous catalyst, ZnO@NPC-Ox-700 can be readily separated from the reaction system by simple filtration. Remarkably, both conversion and selectivity of the catalyst remain almost unchanged during the ten runs of circulation (Figure 3). Moreover, the PXRD pattern of ZnO@NPC-Ox-700 demonstrates the retained structural integrity after recycling (Figure S17).

To further examine the general application of ZnO@NPC-Ox-700 catalyst, various epoxides were investigated for the CO₂ cycloaddition reaction. In consideration of the low boiling point of 1,2-epoxypropane and 1,2-epoxybutane, both of them were converted at relatively low temperatures. All these epoxides with different substituent groups gave good to excellent conversion and high selectivity (Table 2). Owing to the low reaction temperature, the catalytic efficiency was a little lower than

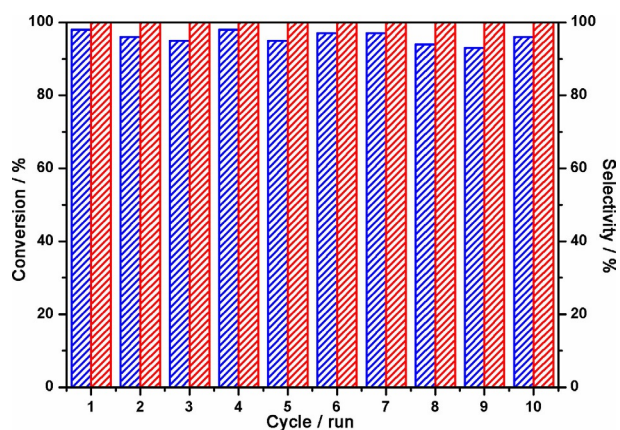


Figure 3. Conversion (blue column) and selectivity (red column) of ZnO@NPC-Ox-700 toward CO₂ cycloaddition with styrene oxide during ten consecutive runs.

Table 2. CO₂ cycloaddition with epoxides substituted with different functional groups over ZnO@NPC-Ox-700.^[a]

Entry	Substrate	T [°C]	t [d]	Con. ^[b] [%]	Sel. ^[b] [%]
1		25	3	85	100
2		45	3	90	100
3		60	1	94	> 99
4		60	1	95	100
5		60	2	> 99	100

[a] Reaction conditions: 1 mmol substrate, 50 mg ZnO@NPC-Ox-700, 0.2 mmol TBAB, 2 mL acetonitrile, 0.1 MPa CO₂. [b] Determined by GC and using *n*-dodecane as a standard.

that of styrene oxide (entries 1–2). The cycloaddition of all the epoxides with electron-withdrawing substituents (–Cl, –Br, and –OPh) proceeds more efficiently than for styrene oxide (entries 3–5). That is probably because the C–O bonds of these substrates are weaker than that of styrene oxide caused by the conjugation between epoxy group and benzene ring.

As mentioned above, extensive efforts have been devoted to CO₂ cycloaddition reaction.^[2c,d,g,5] Therefore, it would be natural to compare the catalytic performance of ZnO@NPC-Ox-700 with the corresponding systems involving catalysts with porous carbons, ZIFs and MOFs, etc. As shown in Table S4, the reactions over porous carbons, ZIFs, and MOFs mostly require harsh conditions and high energy (relatively high temperature and/or CO₂ pressure). Moreover, some catalysts like MOF-5 are sensitive to moisture/water or/and a few ligands of MOF catalysts are expensive, which are unfavorable for practical applications. In contrast, ZnO@NPC-Ox-700 based on inexpensive raw materials requires mild catalytic reaction conditions and exhibits high catalytic performance and superb stability (Figure 3 and S17).

On the basis of these catalytic results, we proposed the reaction mechanism as follows: As displayed in Scheme S1 to S3, the C–O bond of the epoxide can be first polarized by the phenolic hydroxyl groups, carboxylic acid or the Zn²⁺ of ZnO (different acid sites).^[8] At the same time, CO₂ can be activated by the pyridinic N or the O^{2–} of ZnO (Lewis base sites).^[6c,8d] Then, the heterolysis of the C–O bond occurs by the nucleophilic attack of the halide anion on the less sterically hindered carbon atom of the epoxide. Subsequently, the carbon atom of CO₂ is attacked nucleophilically by the ring-opened intermediate. Finally, the internal nucleophilic attack of the ring-opened intermediate results in the formation of cyclic carbonate with the regeneration of the catalyst and co-catalyst.

In summary, the ZnO@NPC-Ox (NPC: N-doped porous carbon) composites were rationally synthesized by the pyrolysis of the metal–organic framework ZIF-8 at different temperatures in N₂ atmosphere and subsequently oxidized with a

moderate oxidant, sodium hypochlorite. In contrast to a traditional oxidant like HNO_3 , the moderate oxidation not only results in different functional groups on the surface of carbon but also avoids etching off important components like ZnO, eventually offering the oxidized porous carbon with multiple catalytic sites (ZnO, pyridinic N, hydroxyl, carboxyl, etc.). Based on the synergy of the different types of catalytic sites and the porosity inherited from ZIF-8, the optimized catalyst, ZnO@NPC-Ox-700, exhibits excellent activity, selectivity, stability, and recyclability toward the CO_2 cycloaddition reactions with diverse epoxides under mild conditions. Given the structural diversity and tailorability of MOFs, this synthetic approach would open up an avenue to the design of advanced porous composites involving multiple sites for diverse applications, especially in catalysis.

Experimental Section

Preparation of catalysts

Synthesis of ZIF-8 nanocrystals: ZIF-8 nanocrystals were prepared according to a previous literature report with minor modifications.^[18] Typically, $\text{Zn}(\text{NO}_3)_2 \cdot 6\text{H}_2\text{O}$ (1.68 g, 5.65 mmol) was dissolved in methanol (80 mL). Then a mixture of 2-methylimidazole (3.70 g, 45 mmol) and methanol (80 mL) was added to the above solution and stirred for 24 h at room temperature. The precipitate was separated by centrifugation, then washed with methanol three times, and soaked in fresh methanol for one day. Finally, the ZIF-8 powder was obtained by centrifugation, washed with methanol three times, and dried overnight at 60 °C in vacuum.

Synthesis of ZnO@NPC: The activated ZIF-8 powder (500 mg) was pyrolyzed at different temperatures (700, 800, 900, 1000 °C) for 2 h at a heating rate of 5 °C min⁻¹ under a nitrogen flow of about 60 mL min⁻¹. Finally, the resulting product was obtained by cooling down to room temperature naturally.

Synthesis of ZnO@NPC-Ox: The above-obtained ZnO@NPC (100 mg), deionized water (10 mL), and sodium hypochlorite (14.5% available chlorine, 2.5 mL) were added into a 50 mL round-bottom flask successively. Then, the mixture was stirred at room temperature for 24 h. After that, methanol (30 mL) was added into the reaction system and the oxidized porous composites were obtained by filtration, then washed with methanol for several times, and dried at 60 °C in vacuum.

HNO_3 treatment for ZnO@NPC-700 and ZnO@NPC-Ox-700: Typically, the mixture of ZnO@NPC-700 or ZnO@NPC-Ox-700 (100 mg) and HNO_3 aqueous solution (1 M, 16 mL) was added into a 50 mL round-bottom flask and stirred at 105 °C for 1.5 h. After cooling down to room temperature, the solid was obtained by filtration, then washed with methanol several times, and dried at 60 °C in vacuum.

Synthesis of ZnO derived from ZIF-8: The activated ZIF-8 powder (500 mg) was pyrolyzed at 700 °C for 2 h at a heating rate of 5 °C min⁻¹ in air. Finally, ZnO powder was obtained by cooling down to room temperature naturally.

Synthesis of NPC-Ox-700: Typically, ZnO@NPC-Ox-700 (100 mg) was introduced and stirred in HCl aqueous solution (1 M, 20 mL) at room temperature for 6 h. The product (NPC-Ox-700) was obtained by centrifugation, then washed with water and methanol several times, and dried at 60 °C in vacuum.

Synthesis of ZnO@NPC-Ox and ZnO@AC: Typically, the mixture of NPC-Ox-700 or activated carbon (AC, 200 mg), $\text{Zn}(\text{NO}_3)_2 \cdot 6\text{H}_2\text{O}$ (118 mg, 0.396 mmol) (the same Zn^{2+} content as that in ZnO@NPC-Ox-700), and ethanol (1 mL) was stirred at room temperature for 1 h. Then, ethanol was evaporated under vacuum at 70 °C for 1 h and the dried powder was subsequently pyrolyzed at 400 °C for 3 h at a heating rate of 5 °C min⁻¹ under a N_2 flow of ~60 mL min⁻¹. The product was obtained by cooling down to room temperature naturally.

Catalytic performance evaluation

Cycloaddition of CO_2 and epoxide: Typically, a mixture of catalyst (50 mg), TBAB (65 mg, 0.2 mmol), acetonitrile (2 mL), and epoxide (1 mmol) was added into a 5 mL round-bottom flask, which was connected to a CO_2 balloon. Then, the mixture was stirred at 60 °C for 2 days.

Recyclability investigation for ZnO@NPC-Ox-700 catalyst: After the cycloaddition reaction of CO_2 and styrene oxide for 2 days, the catalyst (ZnO@NPC-Ox-700) was separated by filtration, washed with methanol several times, and dried overnight at 60 °C in vacuum. After that, the catalyst was used for another cycloaddition of CO_2 and styrene oxide. This procedure was conducted up to ten times to examine the recyclability of ZnO@NPC-Ox-700.

Acknowledgements

This work was supported by the 973 program (2014CB931803), the NSFC (21371162, 21673213 and 21521001), the State Key Lab of Materials-Oriented Chemical Engineering (KL15-02) and the Recruitment Program of Global Youth Experts.

Keywords: carbon • CO_2 fixation • doping • heterogeneous catalysis • metal-organic frameworks

- [1] a) Z. Zhang, Z.-Z. Yao, S. Xiang, B. Chen, *Energy Environ. Sci.* **2014**, *7*, 2868–2899; b) E. S. Sanz-Pérez, C. R. Murdock, S. A. Didas, C. W. Jones, *Chem. Rev.* **2016**, *116*, 11840–11876.
- [2] a) X. Chang, T. Wang, J. Gong, *Energy Environ. Sci.* **2016**, *9*, 2177–2196; b) J. Qiao, Y. Liu, F. Hong, J. Zhang, *Chem. Soc. Rev.* **2014**, *43*, 631–675; c) G. Sneddon, A. Greenaway, H. H. P. Yiu, *Adv. Energy Mater.* **2014**, *4*, 1301873; d) M. Aresta, A. Dibenedetto, A. Angelini, *Chem. Rev.* **2014**, *114*, 1709–1742; e) H.-Q. Xu, J. Hu, D. Wang, Z. Li, Q. Zhang, Y. Luo, S.-H. Yu, H.-L. Jiang, *J. Am. Chem. Soc.* **2015**, *137*, 13440–13443; f) S. Wang, X. Wang, *Angew. Chem. Int. Ed.* **2016**, *55*, 2308–2320; *Angew. Chem.* **2016**, *128*, 2352–2364; g) J. W. Maina, C. Pozo-Gonzalo, L. Kong, J. Schütz, M. Hillc, L. F. Dumée, *Mater. Horiz.* **2017**, <https://doi.org/10.1039/C6MH00484A>.
- [3] T. Reda, C. M. Plugge, N. J. Abram, J. Hirst, *Proc. Natl. Acad. Sci. USA* **2008**, *105*, 10654–10658.
- [4] a) K. Yamaguchi, K. Ebitani, T. Yoshida, H. Yoshida, K. Kaneda, *J. Am. Chem. Soc.* **1999**, *121*, 4526–4527; b) M. North, R. Pasquale, C. Young, *Green Chem.* **2010**, *12*, 1514–1539; c) Y. Zhang, J. Y. G. Chan, *Energy Environ. Sci.* **2010**, *3*, 408–417; d) X.-B. Lu, D. J. Darensbourg, *Chem. Soc. Rev.* **2012**, *41*, 1462–1484; e) M. H. Beyzavi, C. J. Stephenson, Y. Liu, O. Karagiari, J. T. Hupp, O. K. Farha, *Front. Energy Res.* **2015**, *2*, 63.
- [5] a) H. He, J. A. Perman, G. Zhu, S. Ma, *Small* **2016**, *12*, 6309–6324; b) G. Ji, Z. Yang, H. Zhang, Y. Zhao, B. Yu, Z. Ma, Z. Liu, *Angew. Chem. Int. Ed.* **2016**, *55*, 9685–9689; *Angew. Chem.* **2016**, *128*, 9837–9841; c) Y. Xie, T.-T. Wang, X.-H. Liu, K. Zou, W.-Q. Deng, *Nat. Commun.* **2013**, *4*, 1960; d) J. Liang, R.-P. Chen, X.-Y. Wang, T.-T. Liu, X.-S. Wang, Y.-B. Huang, R. Cao, *Chem. Sci.* **2017**, *8*, 1570–1575; e) J. Tharun, K.-M. Bhin, R. Roshan, D.-W. Kim, A. C. Kathalikkattil, R. Babu, H. Y. Ahn, Y. S. Wonc, D.-W. Park, *Green*

- Chem.* **2016**, *18*, 2479–2487; f) R. R. Kuruppathparambil, R. Babu, H. M. Jeong, G.-Y. Hwang, G. S. Jeong, M.-I. Kim, D.-W. Kim, D.-W. Park, *Green Chem.* **2016**, *18*, 6349–6356; g) C. M. Miralda, E. E. Macias, M. Zhu, P. Ratnasamy, M. A. Carreon, *ACS Catal.* **2012**, *2*, 180–183; h) M. H. Beyzavi, R. C. Klet, S. Tussupbayev, J. Borycz, N. A. Vermeulen, C. J. Cramer, J. F. Stoddart, J. T. Hupp, O. K. Farha, *J. Am. Chem. Soc.* **2014**, *136*, 15861–15864.
- [6] a) X. Ma, B. Zou, M. Cao, S.-L. Chen, C. Hu, *J. Mater. Chem. A* **2014**, *2*, 18360–18366; b) T. Toyao, M. Fujiwaki, K. Miyahara, T.-H. Kim, Y. Horiuchi, M. Matsuoka, *ChemSusChem* **2015**, *8*, 3905–3912; c) R. A. Molla, A. Iqbal, K. Ghosh, M. Islam, *ChemistrySelect* **2016**, *1*, 3100–3107; d) G. Kaur, R. K. Rai, D. Tyagi, X. Yao, P.-Z. Li, X.-C. Yang, Y. Zhao, Q. Xu, S. K. Singh, *J. Mater. Chem. A* **2016**, *4*, 14932–14938; e) S. Gadipelli, Z. X. Guo, *ChemSusChem* **2015**, *8*, 2123–2132; f) K. Shen, X. Chen, J. Chen, Y. Li, *ACS Catal.* **2016**, *6*, 5887–5903.
- [7] a) J.-R. Li, Y. Ma, M. C. McCarthy, J. Sculley, J. Yu, H.-K. Jeong, P. B. Balbucena, H.-C. Zhou, *Coord. Chem. Rev.* **2011**, *255*, 1791–1823; b) J. Wang, L. Huang, R. Yang, Z. Zhang, J. Wu, Y. Gao, Q. Wang, D. O'Hare, Z. Zhong, *Energy Environ. Sci.* **2014**, *7*, 3478–3518; c) Z.-R. Jiang, H. Wang, Y. Hu, J. Lu, H.-L. Jiang, *ChemSusChem* **2015**, *8*, 878–885.
- [8] a) X.-L. Meng, Y. Nie, J. Sun, W.-G. Cheng, J.-Q. Wang, H.-Y. He, S.-J. Zhang, *Green Chem.* **2014**, *16*, 2771–2778; b) M. Ding, H.-L. Jiang, *Chem. Commun.* **2016**, *52*, 12294–12297; c) Y. Zhang, S. Yin, S. Luo, C. T. Au, *Ind. Eng. Chem. Res.* **2012**, *51*, 3951–3957; d) M. Ramin, N. V. Vegten, J.-D. Grunwaldt, A. Baiker, *J. Mol. Catal. A* **2006**, *258*, 165–171; e) J. Kim, S.-N. Kim, H.-G. Jang, G. Seo, W.-S. Ahn, *Appl. Catal. A* **2013**, *453*, 175–180; f) W. Zhang, Q. Wang, H. Wu, P. Wu, M. He, *Green Chem.* **2014**, *16*, 4767–4774.
- [9] a) A. Aijaz, N. Fujiwara, Q. Xu, *J. Am. Chem. Soc.* **2014**, *136*, 6790–6793; b) W. Xia, A. Mahmood, R. Zou, Q. Xu, *Energy Environ. Sci.* **2015**, *8*, 1837–1866; c) J.-K. Sun, Q. Xu, *Energy Environ. Sci.* **2014**, *7*, 2071–2100; d) Y. V. Kaneti, J. Tang, R. R. Salunkhe, X. Jiang, A. Yu, K. C.-W. Wu, Y. Yamauchi, *Adv. Mater.* **2017**, <https://doi.org/10.1002/adma.201604898>; e) H.-L. Jiang, B. Liu, Y. Lan, K. Kuratani, T. Akita, H. Shioyama, F. Zong, Q. Xu, *J. Am. Chem. Soc.* **2011**, *133*, 11854–11857; f) Q. Lai, Y. Zhao, Y. Liang, J. He, J. Chen, *Adv. Funct. Mater.* **2016**, *26*, 8334–8344; g) H. Zhong, J. Wang, Y. Zhang, W. Xu, W. Xing, D. Xu, Y. Zhang, X. Zhang, *Angew. Chem. Int. Ed.* **2014**, *53*, 14235–14239; *Angew. Chem.* **2014**, *126*, 14459–14463; h) G. Huang, L. Yang, X. Ma, J. Jiang, S. Yu, H.-L. Jiang, *Chem. Eur. J.* **2016**, *22*, 3470–3477; i) F. Bai, Y. Xia, B. Chen, H. Su, Y. Zhu, *Carbon* **2014**, *79*, 213–226.
- [10] a) K. S. Park, Z. Ni, A. P. Côté, J. Y. Choi, R. Huang, F. J. Uribe-Romo, H. K. Chae, M. O'Keeffe, O. M. Yaghi, *Proc. Natl. Acad. Sci. USA* **2006**, *103*, 10186–10191; b) X.-C. Huang, Y.-Y. Lin, J.-P. Zhang, X.-M. Chen, *Angew. Chem. Int. Ed.* **2006**, *45*, 1557–1559; *Angew. Chem.* **2006**, *118*, 1587–1589.
- [11] A. T. To, P.-W. Chung, A. Katz, *Angew. Chem. Int. Ed.* **2015**, *54*, 11050–11053; *Angew. Chem.* **2015**, *127*, 11202–11205.
- [12] a) Y.-Z. Chen, C. Wang, Z.-Y. Wu, Y. Xiong, Q. Xu, S.-H. Yu, H.-L. Jiang, *Adv. Mater.* **2015**, *27*, 5010–5016; b) P. Zhang, F. Sun, Z. Xiang, Z. Shen, J. Yun, D. Cao, *Energy Environ. Sci.* **2014**, *7*, 442–450; c) D. Zhao, J.-L. Shui, L. R. Grabstanowicz, C. Chen, S. M. Commet, T. Xu, J. Lu, D.-J. Liu, *Adv. Mater.* **2014**, *26*, 1093–1097.
- [13] a) E.-Y. Choi, T. H. Han, J. Hong, J. E. Kim, S. H. Lee, H. W. Kima, S. O. Kim, *J. Mater. Chem.* **2010**, *20*, 1907–1912; b) M. Acik, G. Lee, C. Mattevi, M. Chhowalla, K. Cho, Y. J. Chabal, *Nat. Mater.* **2010**, *9*, 840–845; c) W. E. Barnett, J. C. Mckenna, *J. Chem. Soc. Chem. Commun.* **1971**, 551–552; d) H. Guo, M. Peng, Z. Zhu, L. Sun, *Nanoscale* **2013**, *5*, 9040–9048; e) M. Chmielewski, J. Jurczak, *J. Org. Chem.* **1981**, *46*, 2230–2233; f) C. Xu, X. Shi, A. Ji, L. Shi, C. Zhou, Y. Cui, *PLoS One* **2015**, *10*, e0144842; g) H.-L. Guo, X.-F. Wang, Q.-Y. Qian, F.-B. Wang, X.-H. Xia, *ACS Nano* **2009**, *3*, 2653–2659.
- [14] a) Y. Otake, R. G. Jenkins, *Carbon* **1993**, *31*, 109–121; b) P. Vinke, M. van der Eijk, M. Verbree, A. F. Voskamp, H. van Bekkum, *Carbon* **1994**, *32*, 675–686.
- [15] Y.-X. Zhou, Y.-Z. Chen, L. Cao, J. Lu, H.-L. Jiang, *Chem. Commun.* **2015**, *51*, 8292–8295.
- [16] J. Song, Z. Zhang, S. Hu, T. Wu, T. Jiang, B. Han, *Green Chem.* **2009**, *11*, 1031–1036.
- [17] a) D. I. Kolokolov, A. G. Stepanov, H. Jobic, *J. Phys. Chem. C* **2015**, *119*, 27512–27520; b) Q. Yang, Q. Xu, S.-H. Yu, H.-L. Jiang, *Angew. Chem. Int. Ed.* **2016**, *55*, 3685–3689; *Angew. Chem.* **2016**, *128*, 3749–3753.
- [18] S. R. Venna, J. B. Jasinski, M. A. Carreon, *J. Am. Chem. Soc.* **2010**, *132*, 18030–18033.

 Manuscript received: February 10, 2017

Revised: March 11, 2017

Accepted Article published: March 21, 2017

Final Article published: April 11, 2017